# Behaviour of sand under the constant shear drained stress path: the role of fines

### QUANYANG DONG\*-and JUN YANG†

This paper presents a specifically designed experimental study aimed at exploring the role of fines in altering the behaviour of sand under a constant shear drained (CSD) stress path. The novelty of this study includes that the interplay of several key factors (fines shape, fines content, void ratio) was investigated systematically and the true constant shear stress condition was fulfilled by means of an advanced servo system, which allowed the entire loading response to be captured. One of the marked findings is that the presence of fines not only alters the onset of instability of loose sand but also affects the deformation development thereafter. Drained instability can be triggered more easily in loose sand mixed with silica fines compared with the sand on its own. At the same quantity of fines, instability can be triggered more easily for sand mixed with rounded fines. However, the effect of fines appears to be marginal for sand at a dense state. For all tested specimens, values of the axial strain rate at instability fall in a narrow range (0.008-0.016%/min), meaning that the axial strain rate can potentially be a useful guide for quantitatively determining the inception of instability under CSD conditions. The stress ratio q/p' at onset of instability under the CSD conditions is also state dependent, as under the undrained conditions.

KEYWORDS: constant shear tests; instability; liquefaction; sands; silts/fines; stress path

### INTRODUCTION

When loose saturated sand is sheared under undrained conditions, it may undergo a dramatic loss of strength and a rapid development of deformation before reaching the plastic limit. This phenomenon, known as static or flow liquefaction, has been extensively studied in the past decades owing to its catastrophic consequences in geotechnical applications (e.g. Casagrande, 1971; Poulos et al., 1985; Sladen et al., 1985; Ishihara, 1993; Yamamuro & Lade, 1997; Doanh & Ibraim, 2000; Yang, 2002; Rahman & Lo, 2012; Lashikari et al., 2017). However, there is a growing concern that static liquefaction can also be initiated under drained conditions, as evidenced by the flowslides of instrumented laboratory slopes (Eckersley, 1990; Wang & Sassa, 2001; Take & Beddoe, 2014) and in documented case histories (e.g. Morgenstern et al., 2016). Such drained failures are thought to be caused by a reduction in mean effective stress associated with rising water table or redistribution of pore-water pressure due to rainfall infiltration, irrigation or even snowmelt (Anderson & Riemer, 1995; Leroueil, 2001). The changes of stress state of the soil elements in these situations can be mimicked by a constant shear drained (CSD) stress path (Brand, 1981; Sasitharan et al., 1993; Anderson & Riemer, 1995). Since this stress path is rather different from that of the conventional undrained triaxial tests, there is increasing interest in soil behaviour under CSD conditions (Zhu & Anderson, 1998; Gajo et al., 2000; Chu et al., 2003; Daouadji et al., 2010;

Junaideen et al., 2010; Monkul et al., 2011; Dong et al., 2016; Rabbi et al., 2019; Fanni et al., 2022; Reid et al., 2024; Fotovvat et al., 2024).

Compared with the large volume of undrained triaxial tests, the number of CSD tests in the current literature is, however, very limited, and the findings are also divergent. Several studies have indicated that loss of stability can occur for loose sand specimens under the CSD stress path (Junaideen et al., 2010; Chu et al., 2012), whereas several others have suggested that for any drained stress paths a loose saturated sand specimen can remain stable prior to the classic plastic limit (Monkul et al., 2011). What criterion should be used to determine the initiation of instability is another concern (Alipour & Lashkari, 2018; Rabbi et al., 2019). These discrepancies provide evidence of the complexity of soil behaviour under the CSD stress path; they also cause conceptual difficulties with reference to the existing theories for the analysis of liquefaction and instability problems (Chen & Yang, 2024). One of the reasons for this situation is the difficulty and uncertainty involved in laboratory CSD tests. It has been observed in many CSD tests that the deviatoric stress q was not strictly constant - an example is shown in Fig. 1. The variation of q can be due to the fixed connection between the top cap and the loading ram in the apparatus used, such that the transmitted axial load is affected by decreasing confining pressure (Skopek et al., 1994). Several studies have attempted to maintain a constant axial load during the CSD test, but the lack of cross-sectional area correction or the lack of responsiveness of triaxial static load frames may cause a decreased deviatoric stress (Monkul et al., 2011; Rabbi et al., 2019). There are concerns that the results obtained from such tests may not represent the true CSD behaviour. The importance of maintaining a constant q in CSD tests in relation to the detection of onset of instability using Hill's stability criterion has been discussed in Chen & Yang (2024).

In the present study, the true constant shear stress (CSD) conditions were achieved by means of an advanced servo control and a systematic experimental programme was carried out

Manuscript received 6 January 2024; revised manuscript accepted 6 September 2024.

Discussion on this paper closes 1 December 2025; for further details see p. ii.

<sup>\*</sup> Formerly Department of Civil Engineering, The University of Hong Kong, Hong Kong; now Wenzhou University, Wenzhou, P. R. China

<sup>†</sup> Department of Civil Engineering, The University of Hong Kong, Hong Kong (Orcid:0000-0002-0250-5809).

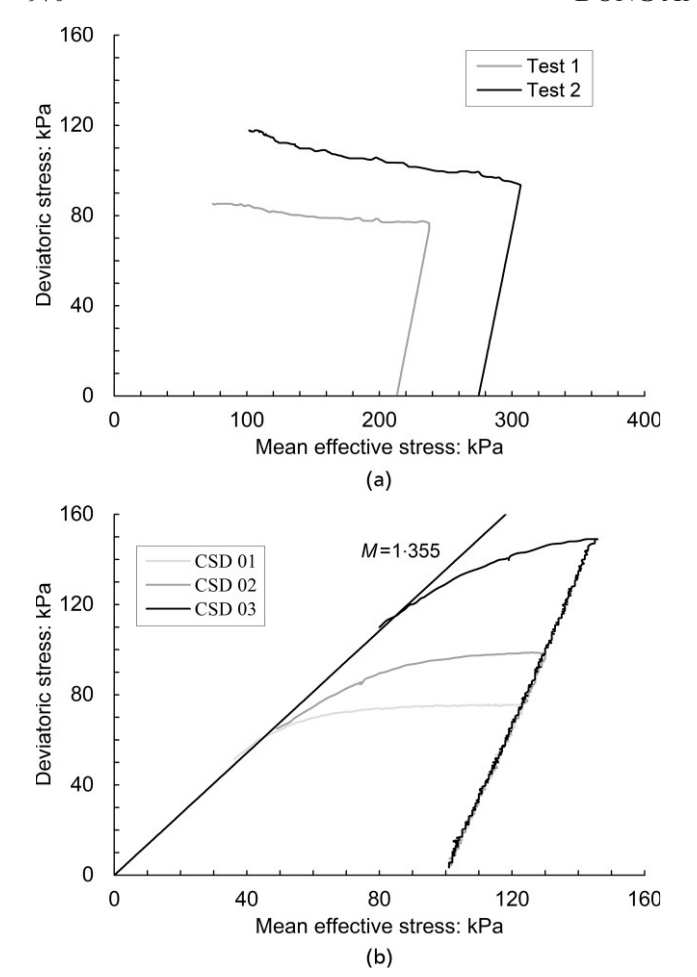


Fig. 1. Variation of deviatoric stress in constant shear drained (CSD) tests: (a) after Skopek *et al.*, 1994; (b) after Rabbi *et al.*, 2019

to investigate the CSD behaviour of sand at both loose and dense states. The experimental set-up allowed the entry response (before and after the onset of instability) along the CSD stress path to be captured reliably – such information is essential for the development of a constitutive relationship and for the development of a comprehensive understanding of the CSD behaviour. Particular attention was paid to the role of adding fines of different shapes and percentages in the initiation of instability. In most geotechnical applications, sand is usually not clean but contains some quantities of fines – this is particularly the case for waste tailings and hydraulic sand fills. In recent years, catastrophic failures of large tailings dams in the form of flowslides associated with rainfall have frequently occurred (Morgenstern et al., 2016; Reid et al., 2022), underlining the insufficiency of current knowledge and the need for research on the CSD behaviour of sand-fines mixtures. The effect of adding fines on the static liquefaction of sand has been discussed in several studies, mainly based on undrained triaxial tests (Kuerbis et al., 1988; Georgiannou et al., 1990; Lade & Yamamuro, 1997; Thevanayagam et al., 2002). More recently, several studies were conducted to investigate the effect of plastic fines on the behaviour of sand under monotonic and cyclic loading conditions (Goudarzy et al., 2022; Fardad Amini & Yang, 2023; Tafili et al., 2023). Of particular interest is the finding that the undrained shear behaviour and collapsibility of sand-fines mixtures is highly affected by the shape of added fines (Yang & Wei, 2012) - sand containing rounded fines tends to exhibit higher susceptibility to collapse or liquefaction than sand mixed with angular fines of the same percentage. In this context, a question of considerable interest

arises: What role is played by fines of varying shape and quantity under the CSD stress path?

This paper presents new data from specifically designed experiments on a clean sand mixed with two non-plastic fines of distinct shapes under the true CSD stress path, with the aim to advance the fundamental understanding of the CSD behaviour of granular soils and eventually to contribute to the development of better solutions to the instability problems of large earth structures. The systematic data can also be used for the calibration and validation of advanced constitutive models and discrete-element simulations.

### EXPERIMENTAL PROGRAMME

Testing materials

Toyoura sand, a uniform quartz sand comprising angular and sub-angular particles, was used as host sand in this study. Two non-plastic fines of distinct shapes, angular crushed silica fines and rounded glass beads, were used as additives to produce two types of sand–fines mixtures. Their physical properties are summarised in Table 1 and the grading curves and microscope images are shown in Fig. 2.

## Specimen preparation and saturation

The moist tamping method, in which the sand was premixed to a moisture content of 5% with the undercompaction technique, was used to prepare the samples. This method was chosen because it is able to produce specimens with a very wide range of density and has the advantage of preventing segregation (Yang & Wei, 2012). The nominal dimension of specimens was 50 mm dia. and 100 mm high. All specimens were saturated in two stages: initially by flushing the specimen with carbon dioxide and de-aired water, and then by applying back-pressure. Specimens with a *B*-value greater than 0.96 were considered saturated.

# Test series

After saturation, each specimen was isotropically consolidated to the target initial mean effective stress, then was brought to a predetermined stress state (i.e.  $p' = 240 \,\mathrm{kPa}$  and  $q = 120 \,\mathrm{kPa}$ ) under the conventional drained triaxial path, after which the CSD stress path was commenced.

A wide range of void ratios was considered, from loose  $(e_{\rm d}=0.951)$  to dense  $(e_{\rm d}=0.745)$ . Here,  $e_{\rm d}$  represents the void ratio prior to applying the CSD stress path. Given the important effect of void ratio, two methods were used to determine the void ratios of the specimens, as suggested by Yang & Wei (2012). The first method was based on the measurements of the initial void ratio during preparation and the volumetric strain that the specimen underwent during consolidation. The second method was base on the measurement of the water content at the end of the test. It has been shown that the two methods can give a reasonably good agreement (Yang & Wei, 2012). For mixtures with high fines content and high compressibility, the second method is recommended. In this study, two percentages of fines, that is 5% and 10%, were considered. Cases of higher fines contents will be studied in future. For convenience of discussion, the abbreviation TS stands for Toyoura sand, TSS(5) stands for Toyoura sand mixed with 5% silica fines and TG(10) stands for Toyoura sand mixed with 10% glass beads. The testing programme is summarised in Table 2.

Table 1. Physical properties of test materials

Materials	$G_{\mathrm{s}}$	D <sub>50</sub> : μm	$C_{ m u}$	$e_{ m max}$	$e_{ m min}$
Toyoura sand	2.65	201.2	1.31	0.977	0.597
Crushed silica Glass beads	2·68 2·65	24·1 37·4	2·63 2·34	_ _	<u> </u>
Shabb beads	1 2 03	] 3/ 4	2 3 1		

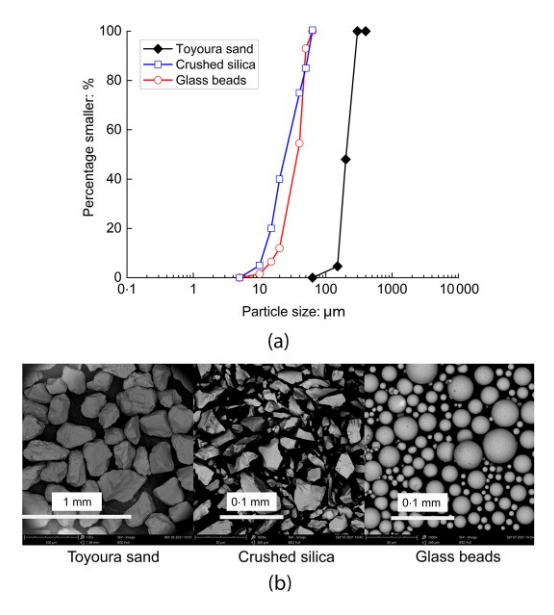


Fig. 2. Test materials: (a) particle size distribution curves; (b) microscope images

# TESTING APPARATUS AND CSD STRESS PATH Testing apparatus

All the CSD tests were performed by a triaxial apparatus, which was equipped with an advanced servo control to strictly maintain the constant deviatoric stress path. Both the deviatoric stress and confining pressure could be varied accurately and independently. The axial stress was applied by way of a servo-loading system, while the confining pressure was supplied through air pressure. The digital pressure–volume controller (DPVC) was used to measure the volume change of the specimen, and updated the specimen's dimensions with the axial displacement measurement so that the axial load could be adjusted to keep the deviatoric stress constant accurately. For all tests reported here, the CSD stress path was achieved by reducing the confining pressure without changing the back-pressure.

### CSD stress path

As an example, Fig. 3 shows various measurements during the CSD test of TS-03. After isotropic consolidation of 200 kPa (point A), the specimen was sheared along a drained stress path to a stress state  $p' = 240 \,\mathrm{kPa}$  and  $q = 120 \,\mathrm{kPa}$  (point B). At point B, the CSD stress path was

Table 2. Test series and key results

	Before CSD		At onset of instability					At failure point						
Test ID	$e_{\mathrm{d}}$	p': kPa	q: kPa	$e_{\mathrm{IL}}$	ε <sub>a</sub> : %	ε <sub>v</sub> : %	$d\varepsilon_a/dt$ : %/min	p': kPa	q: kPa	ε <sub>a</sub> : %	ε <sub>ν</sub> : %	$d\varepsilon_a/dt$ : %/min	p': kPa	q: kPa
TS-01	0.951	240.3	120.0	0.951	0.189	-0.028	0.007	175.0	120.0	14.452	1.577	1.264	87.8	116.8
TS-02	0.930	241.4	120.0	0.932	0.263	-0.085	0.013	150.6	119.9	11.318	1.078	0.985	85.6	117.4
TS-03	0.919	241.1	119.8	0.922	0.205	-0.139	0.012	138.9	119.9	8.495	0.622	1.306	88.8	117.4
TS-04	0.903	240.2	120.0	0.910	0.298	-0.190	0.017	120.8	119.5	11.855	-0.083	1.659	83.0	115.4
TS-05	0.826	241.7	120.0	0.832	0.108	-0.310	0.008	95.5	120.3	1.191	-0.695	0.329	80.8	119.0
TS-06	0.754	240.0	120.0	0.762	0.222	-0.403	0.013	82.8	120.2	1.506	-1.286	0.337	68.5	119-2
TSS(5) - 01	0.937	240.1	120.0	0.938	0.399	0.000	0.014	153.0	120.0	20.915	2.386	2.247	84.2	114.0
TSS(5)-02	0.929	239·1	120.0	0.931	0.287	-0.068	0.012	149.4	120.0	16.828	1.992	1.536	83.2	116.1
TSS(5) - 03	0.903	240.3	119.9	0.908	0.433	-0.248	0.036	107.6	119.9	11.190	0.910	1.254	86.2	116.3
TSS(5)-04	0.857	240.0	120.1	0.864	0.209	-0.392	0.013	97.4	120.2	1.053	-0.629	0.228	82.2	119.3
TSS(5) - 05	0.828	241.1	120.0	0.834	0.147	-0.347	0.011	98.0	119-9	0.644	-0.533	0.115	83.7	119.7
TSS(5) - 06	0.749	241.8	120.1	0.758	0.127	-0.506	0.010	80.3	119.8	0.952	-1.161	0.330	66.3	119.0
TSS(10)-01	0.882	239.7	120.1	0.882	0.329	-0.007	0.012	159.7	119.5	15.595	2.453	1.069	84.1	116.8
TSS(10)-02	0.864	240.9	119.9	0.865	0.221	-0.066	0.010	150.8	120.1	13.789	2.114	0.989	86.9	117.3
TSS(10)-03	0.843	239.4	120.0	0.848	0.275	-0.238	0.016	123.5	119.9	14.793	1.162	1.595	81.5	115.5
TSS(10)-04	0.745	242.0	120.2	0.753	0.141	-0.458	0.011	83.9	119.5	0.627	-0.802	0.143	70.4	119.6
TG(5)-01	0.902	240.0	120.1	0.906	0.180	-0.007	0.010	206.5	120.1	17.284	1.232	1.107	102.6	117.3
TG(5)-02	0.893	239.9	119.9	0.894	0.237	0.005	0.010	194.2	119.9	18.408	1.440	1.104	96.7	117.0
TG(5)-03	0.829	240.2	120.0	0.833	0.269	-0.205	0.014	137.1	119.9	18.880	-0.071	1.379	95.5	116.7
TG(5)-04	0.782	242.0	120.0	0.788	0.185	-0.293	0.010	115.9	119.7	0.740	-0.517	0.173	101.6	119-1
TG(10)-01	0.818	239.0	119.9	0.818	0.263	-0.034	0.015	193.5	119.9	18.512	0.909	1.007	104.3	117·4
TG(10)-02	0.810	242.6	120.0	0.812	0.194	-0.103	0.009	168·1	120.0	18.608	1.112	1.269	104.8	117.0
TG(10)-03	0.806	240.7	119.9	0.807	0.297	-0.007	0.012	203.5	119.8	16.330	0.365	1.092	106.8	116.9
TG(10)-04	0.770	240.1	120.1	0.775	0.178	-0.273	0.009	128.7	120.1	16.596	-1.026	1.181	104.2	117.5

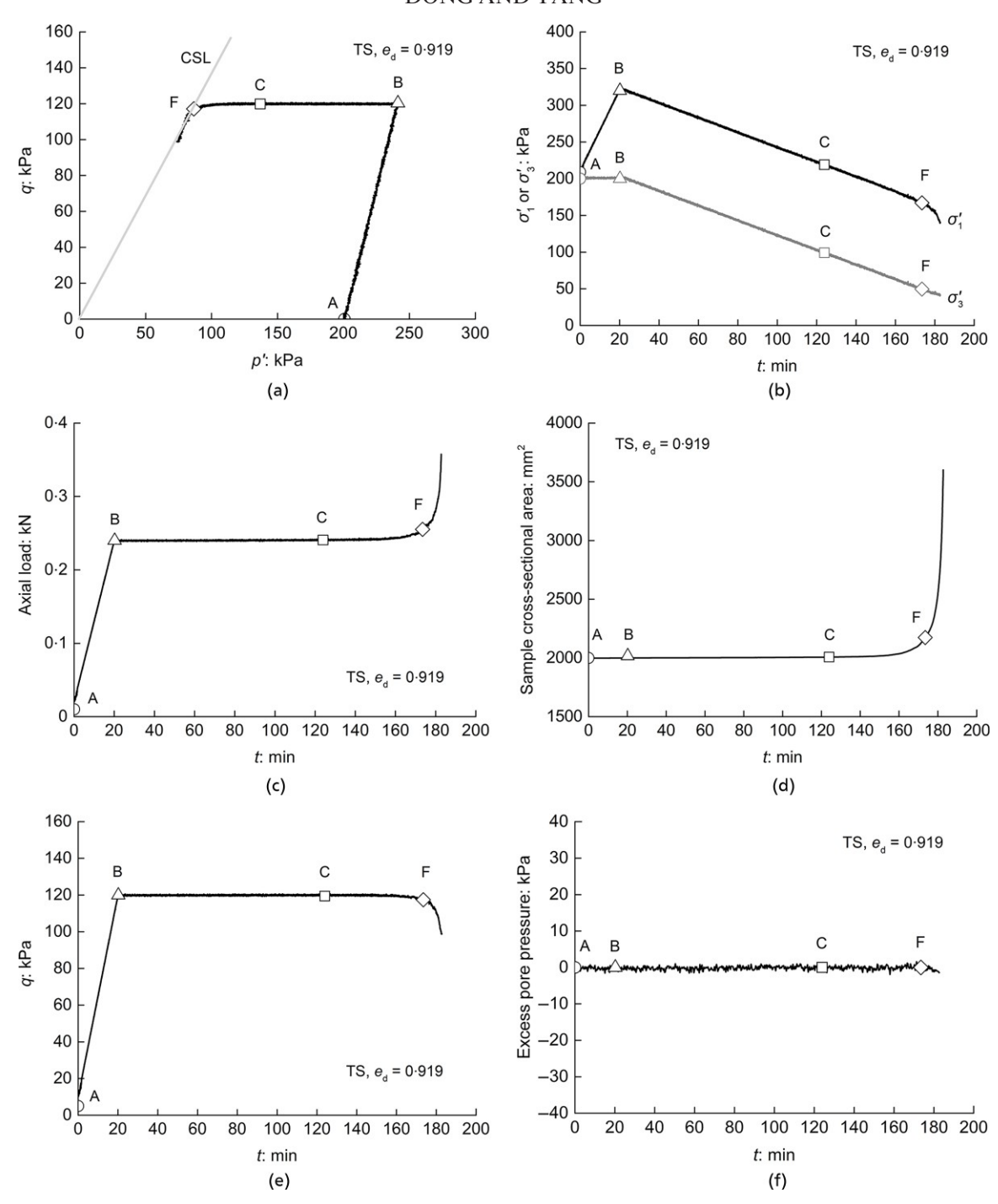
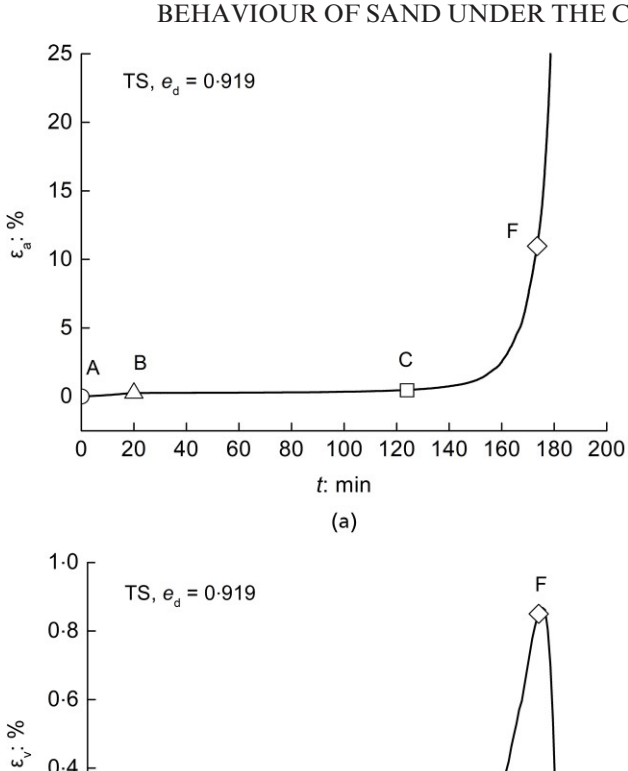


Fig. 3. Various measurements under the CSD stress path (test TS-03): (a) stress path; (b) axial and radial stresses plotted against time; (c) axial load plotted against time; (d) sample cross-sectional area plotted against time; (e) deviatoric stress plotted against time; (f) excess pore water pressure plotted against time

imposed (Fig. 3(a)), which was fulfilled by two steps: first, axial stress and confining pressure were reduced simultaneously at a constant rate of 1 kPa/min (Fig. 3(b)), and second, back-pressure was kept constant using a DPVC during the entire CSD process. The axial load (Fig. 3(c)) was adjusted based on the feedback of volume change measurement to account for the increase in the cross-sectional area (Fig. 3(d)) such that the deviatoric stress was maintained constant accurately. The deviatoric stress was well controlled and its variation was within 3 kPa before failure point F, Fig. 3(e). This value is significantly small compared with previous studies (Skopek *et al.*, 1994; Monkul *et al.*, 2011; Rabbi *et al.*, 2019). After point F, the deviatoric stress dropped dramatically. Here the failure point

corresponds to the maximum stress ratio (Lade & Ibsen, 1997). Note that the reduction rate of confining pressure adopted (1 kPa/min) was slow enough to maintain an ideal drained condition throughout, as confirmed by the excess pore pressure measurement shown in Fig. 3(f).

The time histories of strain measurements for test TS-03 are presented in Fig. 4. Note that the axial strain and volumetric strain generated from point B to C are relatively small, being 0·19% and -0·14%, respectively, Figs 4(a) and 4(b). Here, negative volumetric strain represents a dilative response. Immediately after point B, the volumetric strain decreases as the specimen dilates because of the decrease in the mean effective stress. However, after point C both axial and volumetric strains develop rapidly. By any standards, this



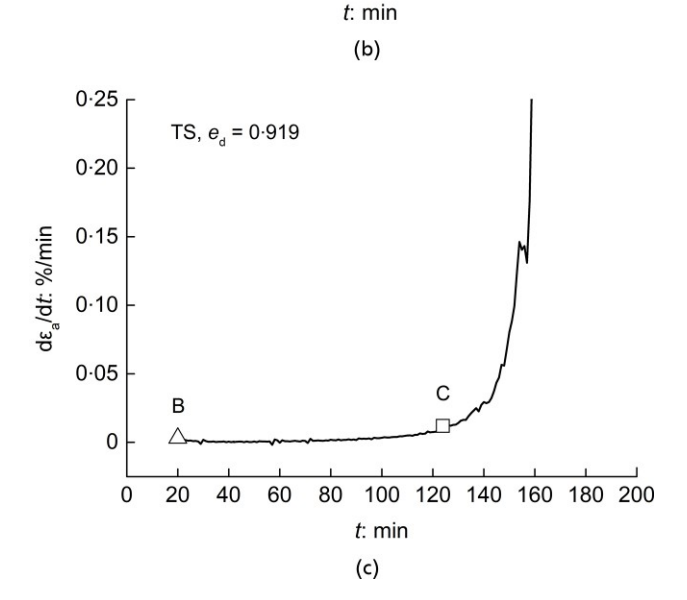
В

40 60 80

0.2

0

0 20



100

120 140 160 180 200

Fig. 4. Time histories of strain measurements of test TS-03: (a) axial strain plotted against time; (b) volumetric strain plotted against time; (c) axial strain rate plotted against time

rapid development of large deformation is not acceptable in geotechnical applications. It is therefore reasonable to assume that the accelerating increase in axial strain (point C) signifies the onset of instability, similarly to that of Chu *et al.* (2012) and Junaideen *et al.* (2010). This is confirmed in Fig. 4(c), where the axial strain rate is plotted as a function of time. It is worth noting, however, that the deviatoric stress after point C does not decrease dramatically until reaching point F under

the CSD condition, Figs 3(a) and 3(c). This is distinctly different from the behaviour of loose sand subjected to undrained triaxial compression.

# TEST RESULTS AND DISCUSSION

Behaviour of sand mixed with crushed silica fines

Figure 5 compares the responses of TS and TSS(5) under the CSD stress path. Both specimens have a similar void ratio ( $e_d = \sim 0.930$ ). The CSD stress path and the development of axial strain with time are shown in Figs 5(a) and 5(b), respectively. The evolution of axial strain rate ( $d\varepsilon_a/dt$ ) and the evolution of volumetric strain with time are shown in Figs 5(c) and 5(d), respectively. The instability and failure points are marked as point C/C' and point F/F' for TS and TSS(5) specimens, respectively. It is noted that the axial strain and volumetric strain generated in TS and TSS(5) specimens are almost coincident until point C/C', implying a minor effect of adding 5% silica fines on the onset of instability as compared with the base sand on its own. Both specimens lost stability at  $\sim 90 \, \text{min}$  (Fig. 5(c)).

However, the two specimens exhibit somehow different developments of axial and volumetric strains upon the onset of instability. The TSS(5) specimen shows a faster development in both axial and volumetric strains, around 17% and 2% at failure point, respectively. By comparison, the TS specimen reaches an axial strain of 11% and a volumetric strain of 1% at the failure point. Similar observations were obtained on another pair of TS and TSS(5) specimens at the void ratio of about 0.903, as shown later.

When the content of silica fines is increased to 10%, a marked change in deformation behaviour is observed, as shown in Fig. 6. Instability was triggered notably earlier in TSS(10) specimen than in TSS(5) specimen, Fig. 6(c). Of particular interest is the effect of fines content on the volumetric response, as shown in Fig. 6(d): the TSS(5) specimen undergoes dilation during the entire CSD stress path whereas the TSS(10) specimen exhibits a transition in volumetric response before and after the onset of instability (i.e. from dilation to contraction). This different response is considered reasonable as the TSS(10) specimen was at a looser state than the TSS(5) specimen. In this regard, the onset of instability in TSS(10) complies with Hill's criterion in terms of the second-order work (Chen & Yang, 2024), whereas that of TSS(5) does not.

Another interesting issue is the effect of adding fines on the CSD behaviour of sand at dense state as compared with the case of loose state. Fig. 7 presents test results of three specimens TS, TSS(5) and TSS(10) at the void ratio of  $\sim$ 0.750, where the stress path is compared in Fig. 7(a), the axial strain development is compared in Fig. 7(b) and the volumetric strain evolution is compared in Fig. 7(d). The time histories of the axial strain rate of all three specimens are shown in Fig. 7(c). A notable feature of these plots is that, in contrast to the case of loose state, adding silica fines either at 5% or 10% imposes almost negligible impact on the behaviour. For all three specimens, rapid development of axial strain occurs almost at the same time and a dilative response is observed throughout the stress path regardless of the presence of fines. Whether the finding holds for higher fines content, say 20% or 30%, requires further experiments and investigation.

Behaviour of sand mixed with glass beads

Now, it is interesting to examine the effect of particle shape of added fines under the CSD conditions. Fig. 8

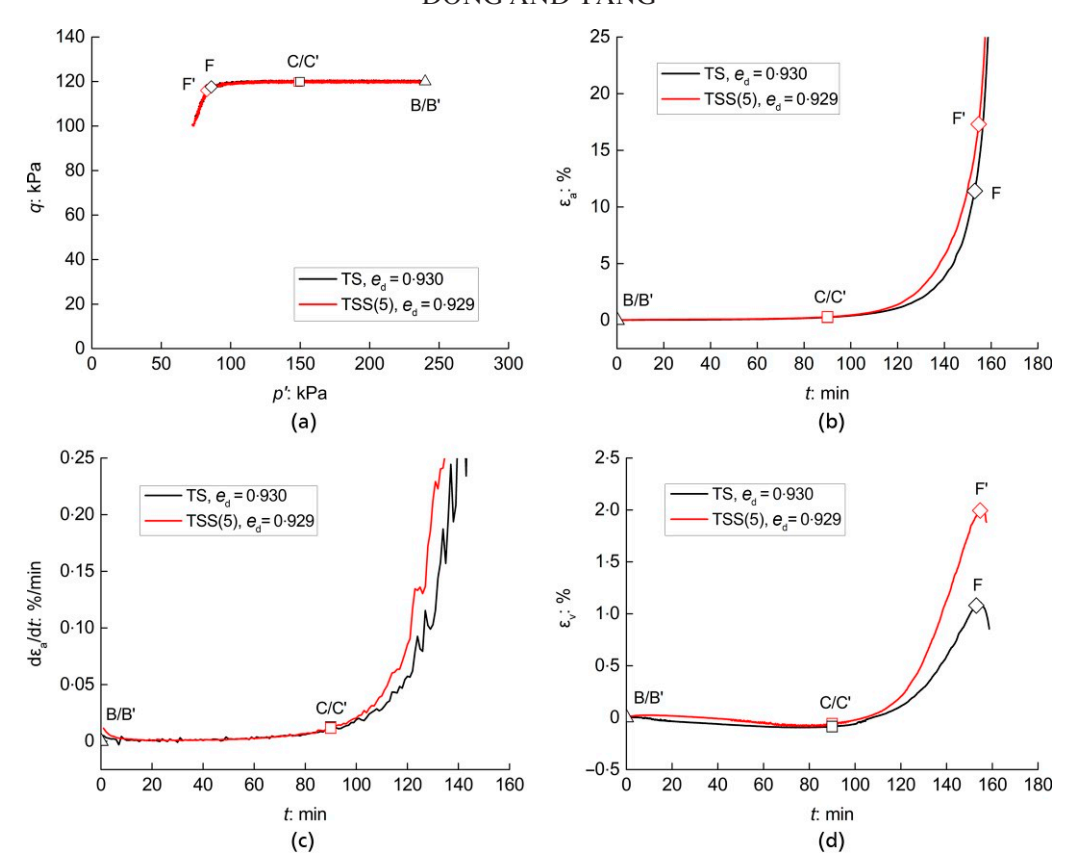


Fig. 5. CSD behaviour of sand modified by addition of crushed silica fines ( $e_d \approx 0.930$ ): (a) stress path; (b) axial strain plotted against time; (c) axial strain rate plotted against time; (d) volumetric strain plotted against time

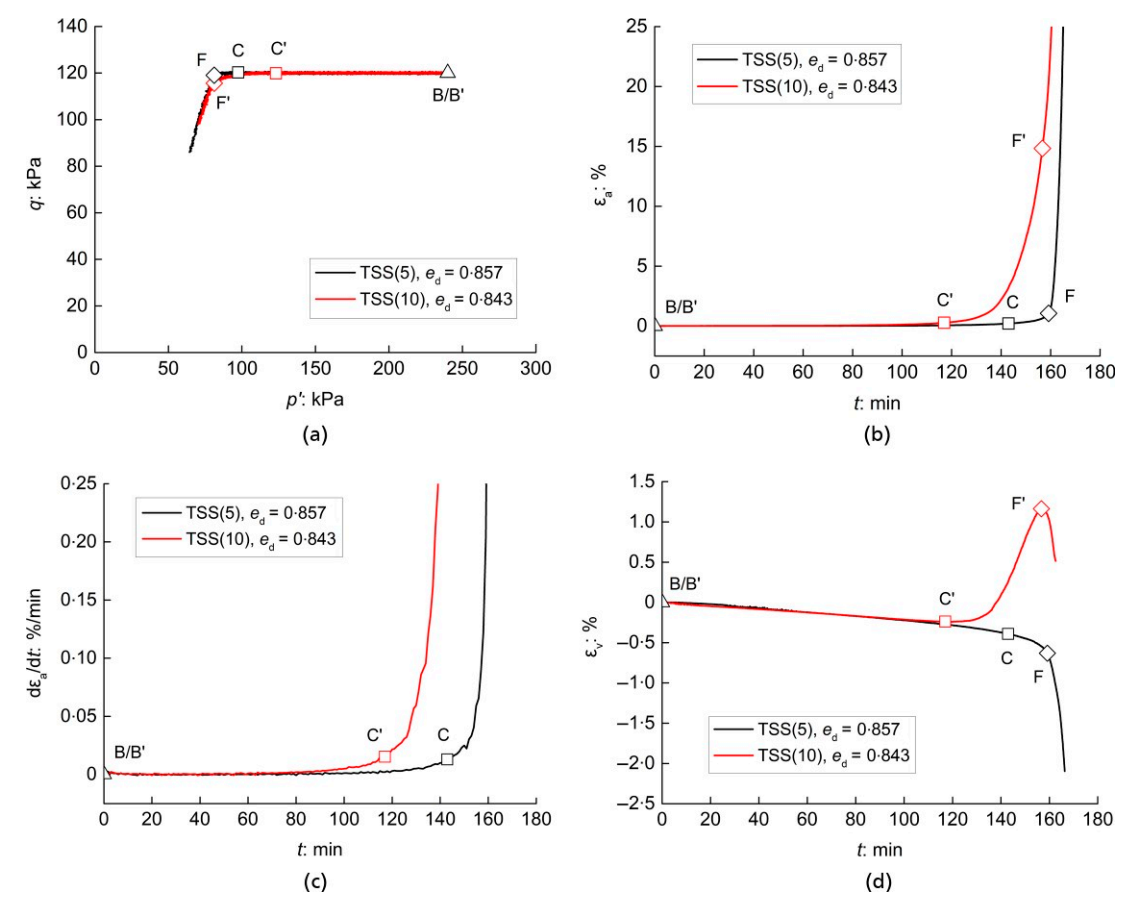


Fig. 6. CSD behaviour of sand modified by addition of crushed silica of different quantities ( $e_d \approx 0.850$ ): (a) stress path; (b) axial strain rate plotted against time; (c) axial strain plotted against time; (d) volumetric strain plotted against time

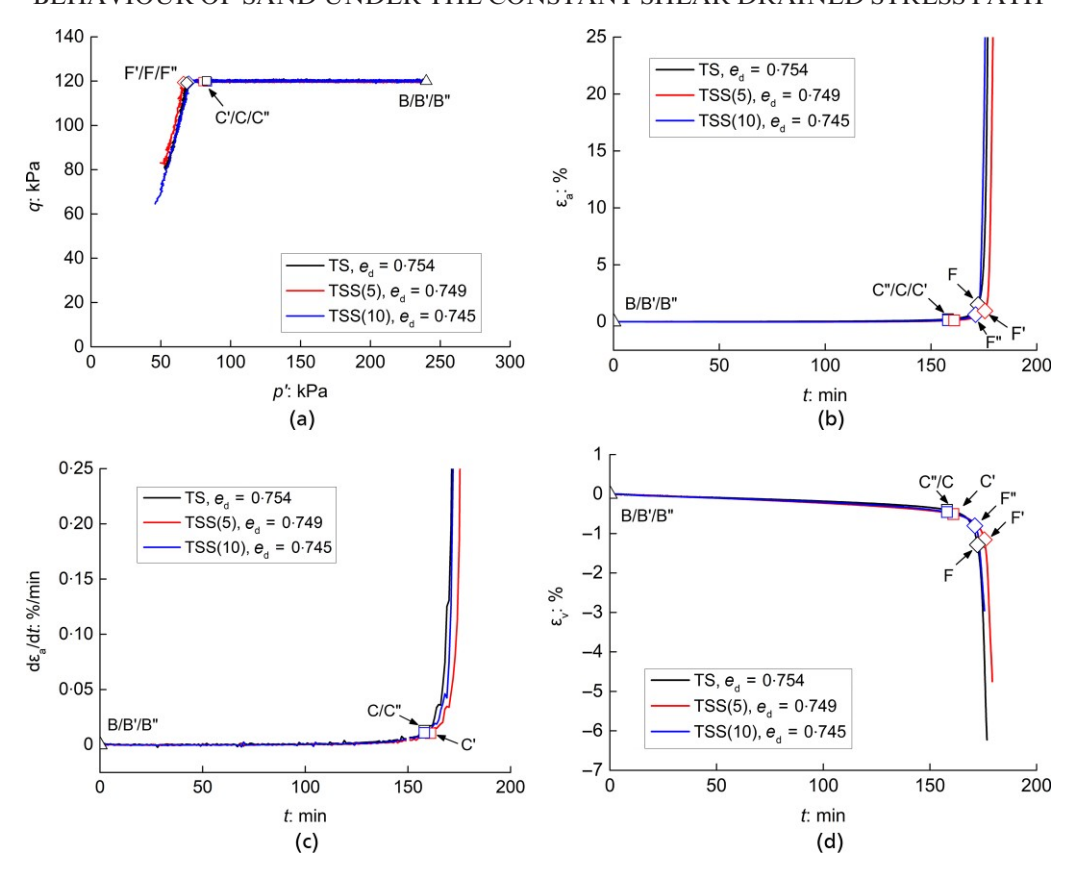


Fig. 7. CSD behaviour of sand modified by addition of crushed silica of different quantities ( $e_d \approx 0.750$ ): (a) stress path; (b) axial strain plotted against time; (c) axial strain rate plotted against time; (d) volumetric strain plotted against time

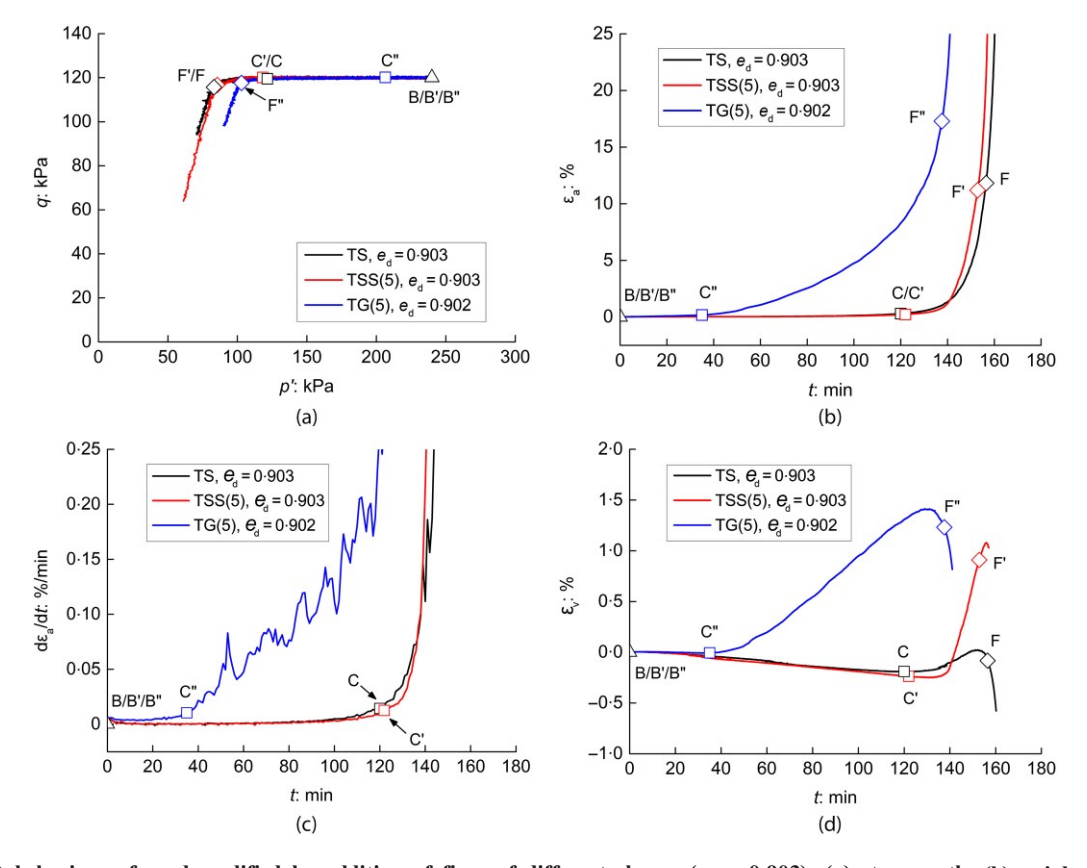


Fig. 8. CSD behaviour of sand modified by addition of fines of different shapes ( $e_d \approx 0.903$ ): (a) stress path; (b) axial strain plotted against time; (c) axial strain rate plotted against time; (d) volumetric strain plotted against time

shows how the behaviour of clean Toyoura sand is altered by the addition of fines of distinct shapes at the void ratio of about 0.903. One may notice that the evolution of axial strain is similar for TSS(5) and TS specimens, as observed in TS and TSS(5) specimens at the void ratio of  $\sim 0.930$ (Fig. 5). However, adding 5% glass beads to Toyoura sand can result in a much earlier onset of instability compared with the TS and TSS(5) specimens, see Figs 8(b) and 8(c). The onset of instability marks a transition in volumetric response from dilative to contractive response, Fig. 8(d). Moreover, the extent of contraction is more significant in TSS(5) and TG(5) specimens as compared with that of the clean sand specimen. Following the onset of instability, the axial strain rate of the TG(5) specimen is less drastic than that of TS and TSS(5) specimens. At the failure point, the TG(5) specimen underwent the largest deformations compared with the other two specimens.

Similar observations can be made in comparing the test results of TG(5), TSS(5) and TS specimens at a void ratio of about 0·828, shown in Fig. 9. These tests confirm that adding 5% glass beads in the clean sand can trigger large deformation earlier as compared with the base sand on its own and the sand mixed with silica fines of the same percentage. It is noteworthy that, at this void ratio, both TS and TSS(5) specimens underwent dilation during the entire CSD stress path, whereas the TG(5) specimen exhibited a transition from dilative to contractive response at the onset of large axial strains. Note that the TG(5) specimen here was at a denser state than TG(5) in Fig. 8, and hence was less contractive.

When Toyoura sand is mixed with glass beads at 10%, the onset of instability can be triggered much earlier, as shown in Fig. 10. The axial strain rate of TG(10) exhibits significant fluctuations upon the onset of instability, but such fluctuations are not observed in TS and TG(5) specimens at the similar void ratio. Interestingly, a sudden drop of deviatoric stress is recorded for TG(10) but the specimen regains capacity thereafter, Fig. 10(a). The phenomenon of fluctuations has also been observed in undrained triaxial tests of clean sand mixed with glass beads (Yang & Wei, 2012; Wei & Yang, 2014) and it is thought to be a reflection of the metastable structure formed. Generally, rounded particles favour rolling and this tends to yield a microstructure that is metastable, whereas angular particles favour sliding and this tends to yield a more stable microstructure.

Characteristics of volumetric response under CSD stress path

Based on the tests on both clean sand and its mixtures over the range of void ratio, two primary patterns of volumetric response are identified for the CSD conditions, as schematically shown in Fig. 11. For a specimen at the loose state, it will undergo a slight dilation before the onset of instability and then exhibit a contractive response towards the failure point. For a specimen at the dense state, however, it will exhibit a dilative response throughout the stress path. Furthermore, three stages in the volumetric response can be identified for the CSD stress path, regardless of loose or dense state. In the first stage (marked as a black line), the

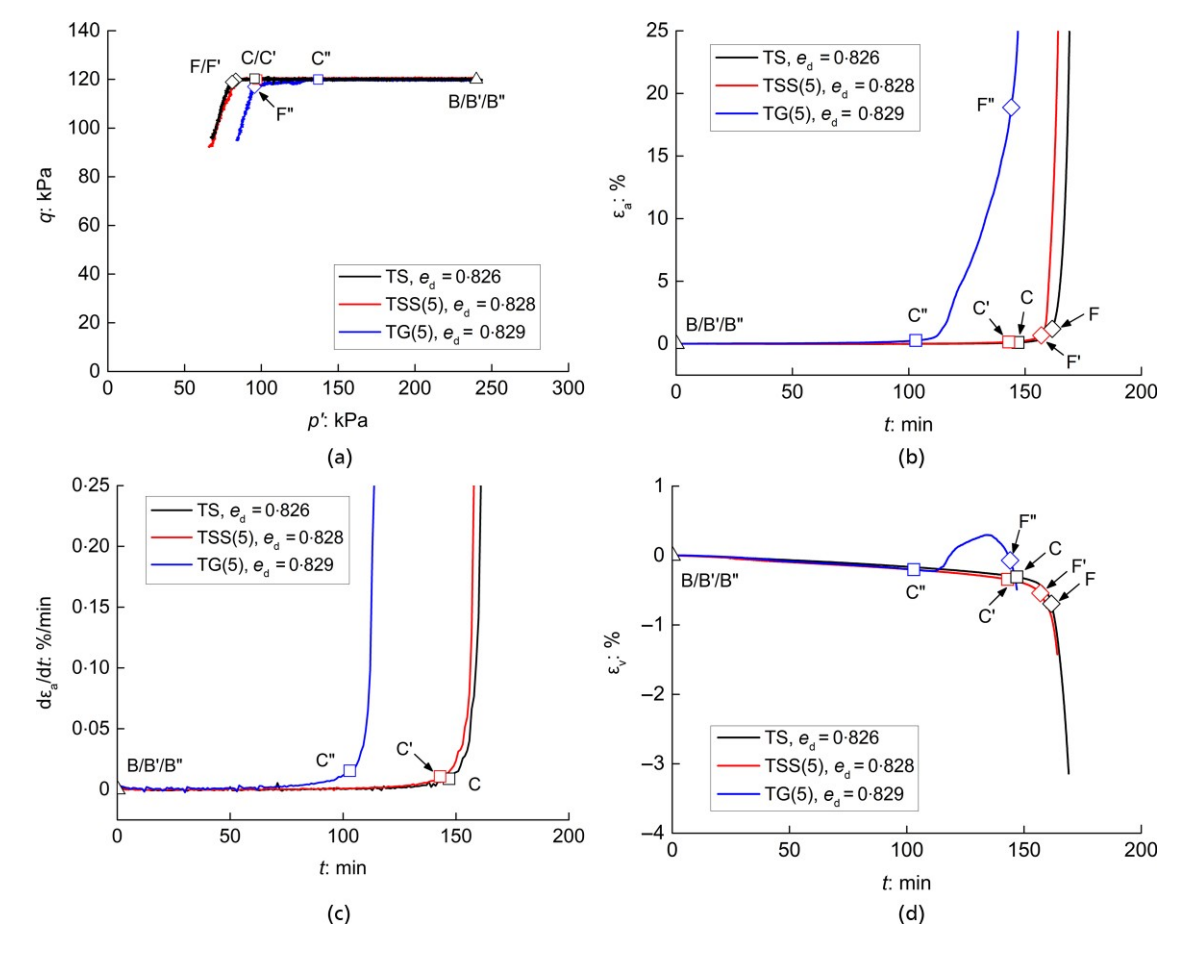


Fig. 9. CSD behaviour of sand modified by addition of fines of different shapes ( $e_d \approx 0.828$ ): (a) stress path; (b) axial strain plotted against time; (c) axial strain rate plotted against time; (d) volumetric strain plotted against time

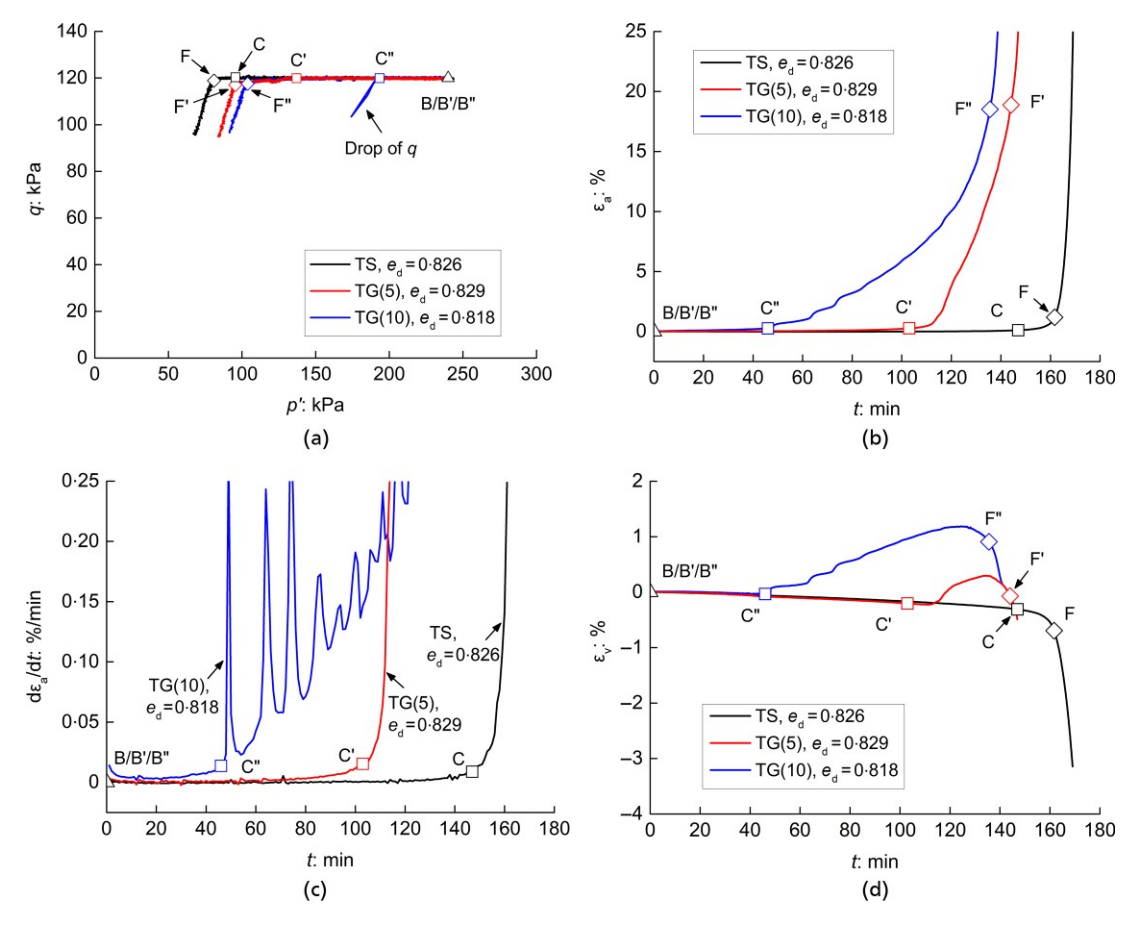


Fig. 10. CSD behaviour of sand modified by addition of glass beads of different quantities ( $e_d \approx 0.826$ ): (a) stress path; (b) axial strain plotted against time; (c) axial strain rate plotted against time; (d) volumetric strain plotted against time

volumetric strain is minimal and the soil behaves as an essentially elastic material. At the beginning of the second stage (marked as a light orange line), the plastic strain begins to develop and then accelerates, leading to the occurrence of instability. In the third stage (marked as a dark orange line), the volumetric strain develops at an almost constant slope. Compared with the conventional triaxial compression test, the CSD test is a kind of unloading test in that the confining pressure is reduced during the test. In this connection, there will be slight dilatancy in the initial stage of loading, even for loose samples. As loading goes on, the increase in stress ratio will cause a contractive response in loose samples and a dilatative response in dense samples, which is similar to the undrained/drained triaxial behaviour. Most recently, Chen & Yang (2024) and Zhang et al. (2023) have presented some new findings about the CSD behaviour compared with triaxial undrained and drained behaviour, from the theoretical and numerical points of view.

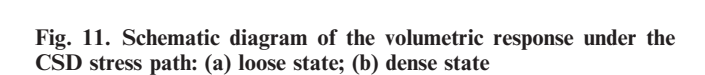
It is noteworthy that all mixed specimens tested in this study have approximately the same slope in the  $\varepsilon_V$ –t or  $\varepsilon_V$ –p' plane in the initial stage. As far as loose specimens are concerned, the slope of the final stage is between 0·033 and 0·048 (%/kPa) for clean Toyoura sand, while it increases to 0·056~0·076 (%/kPa) for the sand mixed with crushed silica fines and decreases to 0·011~0·028 (%/kPa) for the sand mixed with glass beads. These values are summarised in Table 2 for ease of reference. The speed of volumetric deformation in the final stage is in the order of TSS(5) > TS > TG(5), which is schematically shown in Fig. 12. A similar trend is also found in the specimens with 10% fines. These results suggest that adding fines not only alters the onset of instability but also affects the development of deformation thereafter.

Deformations at onset of instability and failure point

As the response of sand at the onset of instability and the failure point is a considerable concern, a detailed analysis of the axial strain and volumetric strain at the two states and axial strain rate at the onset of instability was conducted for all tested specimens. The results of analysis are plotted in Figs 13 and 14, respectively. The plot of Fig. 13(a) shows that the axial strain at the onset of instability falls in a narrow range, between 0.1% and 0.3%, for all tested specimens, and it does not show a clear correlation with the void ratio prior to the CSD stress path. Since the axial strain at instability is relatively small, it would be difficult to use it as the prewarning indicator of instability.

In contrast, the variation of volumetric strain at instability with void ratio, shown in Fig. 13(b), is quite different from that of axial strain. In general, the volumetric strain at instability decreases as the void ratio decreases, meaning that much dilation would take place at instability when the specimen becomes denser. For sand specimens mixed with rounded fines (i.e. glass beads), they tend to be less dilative at instability than those mixed with angular fines (i.e. crushed silica fines). When void ratio is reduced to about 0.75 (the lowest tested in the study), the volumetric strain at instability appears to be insensitive to the presence of fines.

As shown before, the axial strain rate can be used as a reasonable indicator of instability. The data of all tests indicate that values of the axial strain rate at instability fall in a narrow range, between 0.008%/min and 0.016%/min, Fig. 13(c). Literature data on strain rates at onset of instability are limited. It is interesting to notice that in the studies of Chu *et al.* (2003) and Rabbi *et al.* (2019), the axial strain rate at instability is approximately 0.015%/min and



(b)

Failure

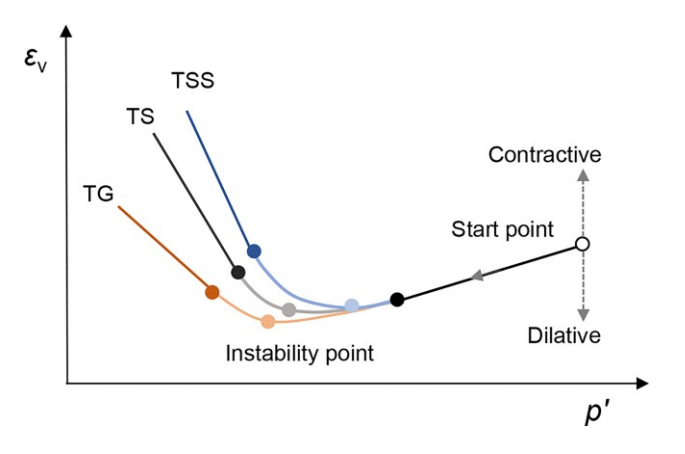
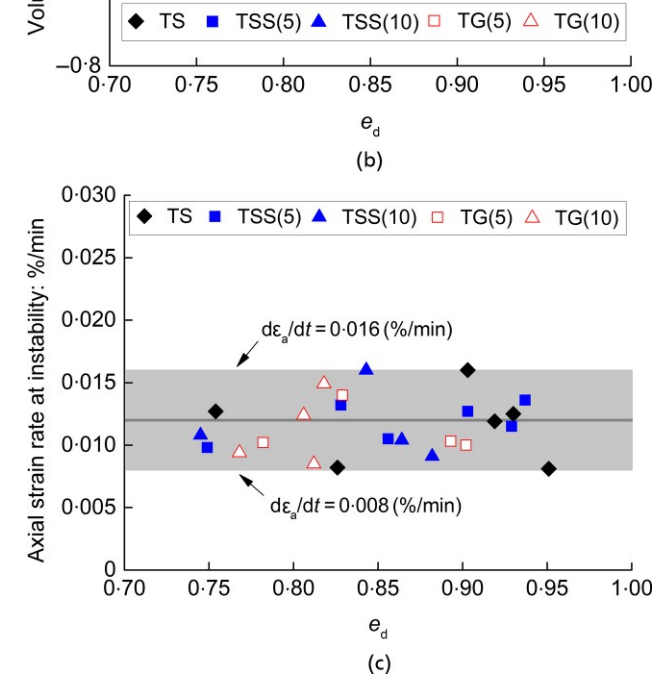


Fig. 12. Schematic diagram of the role of fines shape in altering the volumetric response under the CSD stress path

0.014%/min, respectively. These values fall into the identified strain rate range. As a first approximation, the average value of 0.012%/min can be used to determine quantitatively the instability inception under the CSD conditions. Further experiments on different materials to validate this criterion would be worthwhile.

Figure 14 shows the axial strain and volumetric strains at failure points against void ratio. In general, the axial



0.95

1.00

Fig. 13. Variation with void ratio of (a) axial strain, (b) volumetric strain and (c) axial strain rate at onset of instability

strain can be divided into two zones: the upper one is the contractive zone, in which specimens show a contractive response after onset of instability, whereas the lower one is the dilative zone, in which specimens show a dilative response throughout the CSD stress path. Note that values of axial strain in the contractive zone (8~21%) are significantly larger than those in the dilative zone (0.5 $\sim$ 1.5%). Furthermore, for specimens in the contractive zone, the axial strain tends to increase with increasing void ratio and the

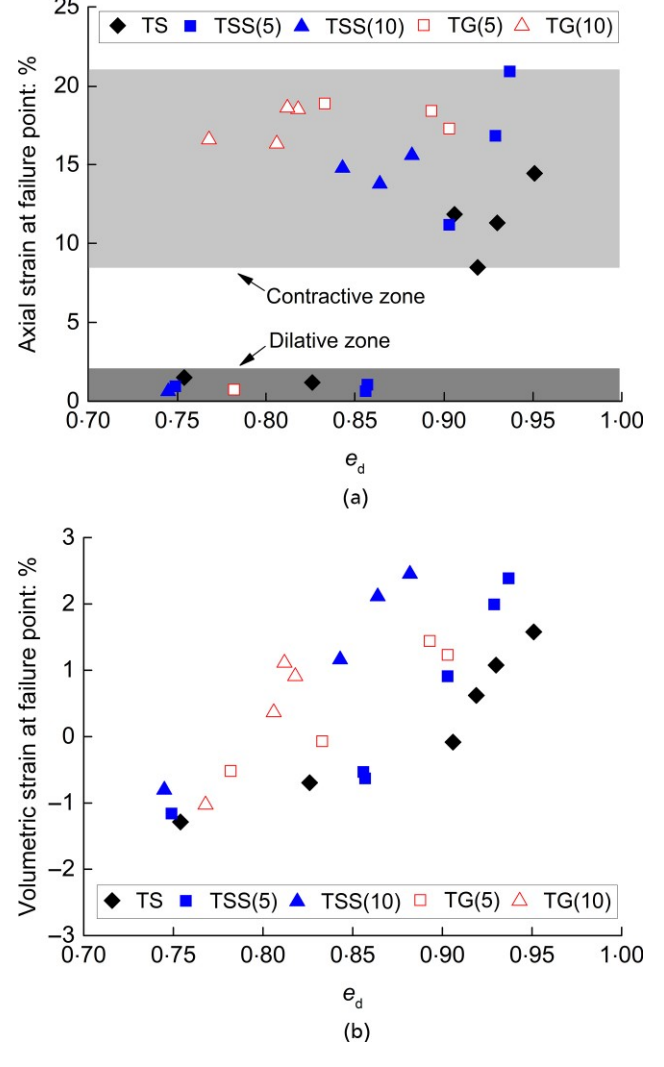


Fig. 14. Variation with void ratio of (a) axial strain and (b) volumetric strain at failure point

trend line tends to shift to the left as the fines content increases. The volumetric strain at the failure point also tends to increase with increasing void ratio, which is similar to that of the volumetric strain at the onset of instability (Fig. 13(b)).

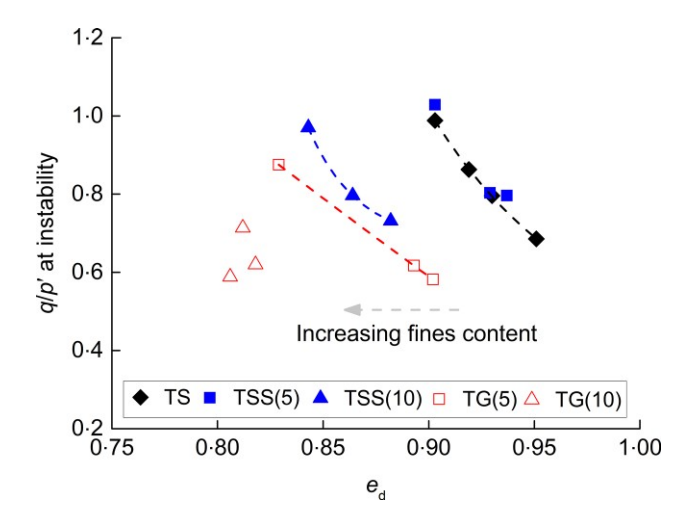


Fig. 15. Variation of the stress ratio at onset of instability with void ratio (loose samples)

Stress ratio at onset of instability

For undrained tests, the line passing through the origin and the peak point on the effective stress path (i.e. the undrained instability state) is defined as the instability line or flow liquefaction line (Vaid & Chern, 1985; Yang, 2002). The slope of this line is useful in characterising the onset of instability or flow liquefaction. For CSD tests here, the onset of instability is determined as the point at which the axial strain rate increases rapidly. For loose specimens which are of particular concern, values of stress ratio q/p' corresponding to this point are shown as a function of void ratio in Fig. 15. Clearly, adding fines of different percentages and shapes has a notable effect. The q/p' curves tend to shift to the left as the quantity of fines increases, suggesting that the instability is triggered at lower stress ratio for sand with higher fines content. Furthermore, given the same quantity of fines, the shift appears to be more significant for sand mixed with rounded glass beads, implying that instability can be triggered more easily. These observations are consistent with those derived from undrained triaxial tests (Yang & Wei, 2012), implying that the exponential function for undrained triaxial tests can also be used to describe the relationship between q/p' and void ratio under the CSD conditions. The theoretical study of Chen & Yang (2024) confirms this finding.

Furthermore, a preliminary analysis of the relation between the stress ratio and the state parameter at onset of instability was conducted, as shown in Fig. 16. Here, the state parameter was estimated using the critical state lines in Yang & Wei (2012) for corresponding materials, and the stress ratio was normalised by the corresponding critical state stress ratio  $(M_{cs})$ . The data in the figure include both loose, contractive samples and dense, dilative samples. Generally, the trend is confirmed for each material that the stress ratio at instability tends to reduce with increasing state parameter; that is, it is easier to trigger instability as the material becomes looser. A similar trend was observed in several other studies (e.g. Fanni et al., 2022). For undrained conditions, the trend has been well confirmed (Yang, 2002). Nevertheless, as the test materials in this study are not exactly the same as the materials in Yang & Wei (2012), there is some uncertainty in the calculation of the state parameter. More experiments are needed to further examine and quantify the relation.

# SUMMARY AND CONCLUSIONS

This paper has presented a specifically designed experimental study which was aimed at exploring the role of fines in

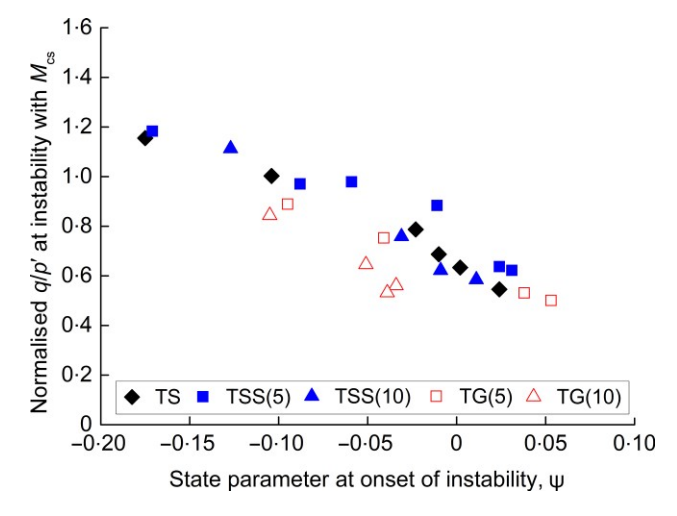


Fig. 16. Normalised stress ratio plotted against state parameter at onset of instability (all samples)

altering the behaviour of sand under the CSD stress path. The true constant shear stress condition was fulfilled by means of an advanced servo system, and the effect of adding fines of different percentages and shapes was investigated. The main results and findings of the study are summarised as follows.

- (a) Under otherwise similar conditions, drained instability can be triggered more easily in a loose sand specimen mixed with 10% silica fines compared with the clean sand specimen on its own and the sand mixed with 5% silica fines. Adding rounded fines (i.e. glass beads) at the same percentage can further increase the susceptibility to instability. This finding suggests the importance of considering both fines content and fines shape in the evaluation of instability of loose sand under CSD conditions.
- (b) The presence of fines not only alters the inception of instability but also affects the development of deformation thereafter. For sand at a loose state, the onset of instability marks a transition in volumetric response from dilation to contraction. Adding angular fines can speed up the volumetric strain following the onset of instability as compared with adding rounded fines of the same quantity.
- (c) For all tests, values of the axial strain at the onset of instability fall in a range of 0·1~0·3%, while values of the axial strain rate at instability fall in a narrow range of 0·008~0·016%/min. As a first approximation, the average axial strain rate of 0·012%/min can be potentially a useful guide for quantitatively determining the onset of instability of sand under CSD conditions.
- (d) The stress ratio q/p' at onset of instability under CSD conditions is state dependent. Drained instability is triggered at a lower stress ratio for sand with higher fines content. At the same quantity of fines, instability can be triggered more easily for sand mixed with rounded fines. The relation proposed for undrained triaxial tests can also be applied to the CSD conditions.
- (e) The influence of fines on the onset of instability as well as the deformation behaviour under the CSD stress path is marked for sand at a loose and contractive state, but it becomes marginal for sand at a dense and dilative state irrespective of the shape and percentage of fines.

The systematic data presented in this paper can serve as a useful reference for further work from a theoretical or experimental point of view. Nevertheless, it should be acknowledged that the soil behaviour under the CSD stress path is complicated and many interesting issues remain to be studied, for example, the case of higher fines content and the effect of plastic fines. The experimental programme to address these issues is being planned, and the results will be reported in future.

## ACKNOWLEDGEMENT

The work was supported by Research Grants Council of Hong Kong (no. 17207923). This support is gratefully acknowledged.

### REFERENCES

- Alipour, M. J. & Lashkari, A. (2018). Sand instability under constant shear drained stress path. *Int. J. Solids Structs* **150**, 66–82, https://doi.org/10.1016/j.ijsolstr.2018.06.003.
- Anderson, S. A. & Riemer, M. F. (1995). Collapse of saturated soil due to reduction in confinement. J. Geotech. Engng 121, No. 2, 216–220.

- Brand, E. W. (1981). Some thoughts on rain-induced slope failures. In *Proceedings of the 10th international conference on soil mechanics and foundation engineering, Stockholm* 3, 373–376.
- Casagrande, A. (1971). On liquefaction phenomena. *Géotechnique* **21**, No. 3, 197–202.
- Chen, Y. & Yang, J. (2024). Initiation of flow liquefaction in granular soil slopes: drained versus undrained conditions. *Acta Geotech.* **19**, No. 1, 39–53, https://doi.org/10.1007/s11440-023-01958-6.
- Chu, J., Leroueil, S. & Leong, W. (2003). Unstable behaviour of sand and its implication for slope instability. *Can. Geotech. J.* **40**, No. 5, 873–885.
- Chu, J., Leong, W. K., Loke, W. L. & Wanatowski, D. (2012). Instability of loose sand under drained conditions. *J. Geotech. Geoenviron. Engng* 138, No. 2, 207–216.
- Daouadji, A., Algali, H., Darve, F. & Zeghloul, A. (2010). Instability in granular materials: experimental evidence of diffuse mode of failure for loose sands. J. Engng Mech. 136, No. 5, 575–588.
- Doanh, T. & Ibraim, E. (2000). Minimum undrained strength of very loose Hostun RF sand in triaxial compression and extension. *Géotechnique* **50**, No. 4, 377–392.
- Dong, Q., Xu, C., Cai, Y., Juang, H., Wang, J., Yang, Z. & Gu, C. (2016). Drained instability in loose granular material. *Int. J. Geomech.* 16, No. 2, 04015043.
- Eckersley, D. (1990). Instrumented laboratory flowslides. *Géotechnique* 40, No. 3, 489–502, https://doi.org/10.1680/geot.1990.40.3.489.
- Fanni, R., Reid, D. & Fourie, A. (2022). Effect of principal stress direction on the instability of sand under the constant shear drained stress path. *Géotechnique* **74**, No. 9, 875–891, https://doi.org/10.1680/jgeot.22.00062.
- Fardad Amini, P. & Yang, J. (2023). Liquefaction susceptibility of clayey sands under saturated andpartially saturated conditions. *Géotechnique* 1–14, https://doi.org/10.1680/jgeot.23.00100.
- Fotovvat, A., Sadrekarimi, A. & Etezad, M. (2024). Instability of gold mine tailings subjected to undrained and drained unloading stress paths. *Géotechnique* 74, No. 2, 174–192.
- Gajo, A., Piffer, L. & Polo, F. D. (2000). Analysis of certain factors affecting the unstable behaviour of saturated loose sand. *Mech. Cohes.-Frict. Mater.* 5, No. 3, 215–237.
- Georgiannou, V., Burland, J. & Hight, D. (1990). The undrained behaviour of clayey sands in triaxial compression and extension. *Géotechnique* **40**, No. 3, 431–449.
- Goudarzy, M., Sarkar, D., Lieske, W. & Wichtmann, T. (2022). Influence of plastic fines content on the liquefaction susceptibility of sands: monotonic loading. *Acta Geotech.* 17, No. 5, 1719–1737, https://doi.org/10.1007/s11440-021-01283-w.
- Ishihara, K. (1993). Liquefaction and flow failure during earthquakes. *Géotechnique* 43, No. 3, 351–451.
- Junaideen, S. M., Tham, L. G., Law, K. T., Dai, F. C. & Lee, C. F. (2010). Behaviour of recompacted residual soils in a constant shear stress path. *Can. Geotech. J.* 47, No. 6, 648–661.
- Kuerbis, R. H., Negussey, D. & Vaid, Y. P. (1988). Effect of gradation and fines content on the undrained response of sand. In *Hydraulic fill structures* (ed. D. J. A. Van Zyl), Geotechnical Special Publication 21, pp. 330–345. Reston, VA, USA: ASCE.
- Lade, P. V. & Ibsen, L. B. (1997). A study of the phase transformation and the characteristic lines of sand behaviour. In *Proceedings of international symposium on deformation and* progressive failure in geomechanics (eds A. Asaoka, T. Adachi and F. Oka), pp. 353–359. Oxford, UK: Elsevier Science Ltd.
- Lade, P. V. & Yamamuro, J. A. (1997). Effects of nonplastic fines on static liquefaction of sands. *Can. Geotech. J.* 34, No. 6, 918–928.
- Lashikari, A., Karimi, A., Fakharian, K. & Kaviani-Hamedani, F. (2017). Prediction of undrained behavior of isotropically and anisotropically consolidated firoozkuh sand: instability and flow liquefaction. *Int. J. Geomech.* 17, No. 10, 04017083.1.
- Leroueil, S. (2001). Natural slopes and cuts: movement and failure mechanisms. *Géotechnique* 51, No. 3, 197–243.
- Monkul, M. M., Yamamuro, J. A. & Lade, P. V. (2011). Failure, instability, and the second work increment in loose silty sand. *Can. Geotech. J.* 48, No. 6, 943–955.

- Morgenstern, N. R., Vick, S. G., Viotti, C. B. & Watts, B. D. (2016). Report on the immediate causes of the failure of the Fundao dam. New York, NY, USA: Cleary Gottlieb Steen and Hamilton LLP.
- Poulos, S. J., Castro, G. & France, J. W. (1985). Liquefaction evaluation procedure. J. Geotech. Engng 111, No. 6, 772–792.
- Rabbi, A. T. M. Z., Rahman, M. M. & Cameron, D. (2019). Critical state study of natural silty sand instability under undrained and constant shear drained path. *Int. J. Geomech.* 19, No. 8, 04019083.
- Rahman, M. & Lo, S. R. (2012). Predicting the onset of static liquefaction of loose sand with fines. *J. Geotech. Geoenviron. Engng* 138, No. 8, 1037–1041.
- Reid, D., Fanni, R. & Fourie, A. (2022). Assessing the undrained strength cross-anisotropy of three tailings types. *Géotechnique Lett.* **12**, No. 1, 1–7.
- Reid, D., Fanni, R. & Fourie, A. (2024). A SHANSEP approach to quantifying the behaviour of clayey soils on a constant shear drained stress path. *Can. Geotech. J.* 61, No. 8, 1517–1540.
- Sasitharan, S., Robertson, P., Sego, D. & Morgenstern, N. (1993). Collapse behavior of sand. *Can. Geotech. J.* **30**, No. 4, 569–577.
- Skopek, P., Morgenstern, N., Robertson, P. & Sego, D. (1994). Collapse of dry sand. *Can. Geotech. J.* **31**, No. 6, 1008–1014.
- Sladen, J. A., D'Hollander, R. D. & Krahn, J. (1985). The liquefaction of sands, a collapse surface approach. *Can. Geotech. J.* 22, No. 4, 564–578, https://doi.org/10.1139/t85-076.
- Tafili, M., Knittel, L., Gauger, V., Wichtmann, T. & Stutz, H. H. (2023). Experimental study on monotonic to high-cyclic behaviour of sand–silt mixtures. *Acta Geotech.* 19, No. 7, 4227–4240, https://doi.org/10.1007/s11440-023-02126-6.

- Take, W. A. & Beddoe, R. (2014). Base liquefaction: a mechanism for shear-induced failure of loose granular slopes. *Can. Geotech. J.* **51**, No. 5, 496–507.
- Thevanayagam, S., Shenthan, T., Mohan, S. & Liang, J. (2002). Undrained fragility of clean sands, silty sands, and sandy silts. *J. Geotech. Geoenviron. Engng* **128**, No. 10, 849–859.
- Vaid, Y. P. & Chern, J. C. (1985). Cyclic and monotonic undrained response of sands. In Advances in the art of testing soils under cyclic loading conditions, proceedings of the ASCE convention, Detroit (ed. V. Khosla), pp. 120–147. New York, NY, USA: ASCE.
- Wang, G. & Sassa, K. (2001). Factors affecting rainfall-induced flow slides in laboratory flume tests. *Géotechnique* 51, No. 7, 587–599.
- Wei, L. M. & Yang, J. (2014). On the role of grain shape in static liquefaction of sand-fines mixtures. Géotechnique 64, No. 9, 740–745.
- Yamamuro, J. A. & Lade, P. V. (1997). Static liquefaction of very loose sand. Can. Geotech. J. 34, No. 6, 905–917.
- Yang, J. (2002). Non-uniqueness of flow liquefaction line for loose sand. *Géotechnique* **52**, No. 10, 757–760.
- Yang, J. & Wei, L. M. (2012). Collapse of loose sand with the addition of fines: the role of particle shape. *Géotechnique* 62, No. 12, 1111–1125.
- Zhang, L., Tang, X. & Yang, J. (2023). Rainfall-induced flowslides of granular soil slopes: insights from grain-scale modeling. *Engng Geol.* 323, 107223.
- Zhu, J.-H. & Anderson, S. (1998). Determination of shear strength of Hawaiian residual soil subjected to rainfall-induced landslides. *Géotechnique* **48**, No. 1, 73–82.